A double-layer of stable coral-like PSi@C(N) anodes for lithium-ion Batteries synthesized from microsilica

Zhao Zhang
Kunming University of Science and Technology
Fengshuo Xi
Kunming University of Science and Technology
Xiuhua Chen
Yunnan University
shaoyuan Li (lsy415808550@163.com)
Kunming University of Science and Technology https://orcid.org/0000-0002-8124-8408
Wenhui Ma
Kunming University of Science and Technology
Yu Lei
xi'an mingde ligong xueyuan: Northwestern Polytechnical University Xi'an Mingde Institute of Technology
Zhao Ding
Wuhan University of Science and Technology
Tao Qu
Kunming University of Science and Technology
Yongnian Dai
Kunming University of Science and Technology
Rong Deng
University of South Wales

Research Article

Keywords: Lithium-ion battery, Porous silicon, Carbon coating, Magnesiothermic reduction, Silicon Anode

Posted Date: April 11th, 2022

DOI: https://doi.org/10.21203/rs.3.rs-1431400/v1

Abstract

With the development of silicon smelting industry, increasing industrial waste (Microsilica) has become a serious concern. From the point of view of environment, it is an important problem how to treat and recycle these microsilica. Silicon (Si) is a promising material for the next generation of lithium-ion batteries anode. Yet, the severe expansion, poor capacity retention or harsh processing technic impede its commercialization path. Herein, a spherical porous silicon were firstly prepared through a magnesiothermic reduction of microsilica, waste powder from photovoltaic silicon production industry. The porous silicon (PSi) was further coated with nitrogen-doped carbon (C(N)) to build a Jellyfish-like PSi@C(N) structure. The PSi@C(N) with uniform interconnected pore channels and nitrogen-doped carbon layer, not only enhances the Li^+ ions transport, but also accommodates extreme volumetric changes of Si during the charge/discharge. The PSi@C(N) electrodes delivered a reversible capacity of 803.92 mAh g^{-1} after 300 cycles at 1000 mA g^{-1} and exhibited 18.6% expansion rate. This study not only provides the rational design of a high-performance porous silicon anode, but also adds a new perspective for the high-value usage of microsilica in semiconductor and photovoltaic industries.

Introduction

In recent years, mankind has made efforts to achieve global carbon neutrality. With the promotion of ecological-environmental protection concept and the development of energy-storage-technology, clean energy has become an important measure to solve global environmental problems, and environmental-energy-materials have become a crucial component (M. Armand et al., 2008). During the high-temperature smelting of industrial silicon and ferrosilicon, a huge volume of dust, which contains significant amount of microsilica ranging from 0.1 to 10 μm (Fig. S1), are collected by the dust collecting device when the vapors are discharged through the flue (Y. Qing et al., 2007, C.S. Poon et al., 2006). As known, the direct discharge of dust to the atmosphere is blamed for polluting environment and causing health problems. Since the dust is mainly consisted by SiO_2 (with purity above 98%,), and negligible amount of metal impurities (Table S1), which can be used as additive to the concretes (D. Prasanya et al., 2016, Wongkeo H et al.,2019, Yazıcı et al., 2008, F Pelisser et al., 2011), or precursors for nanostructured silicon anode materials for LIBs.

The requirements of extending range of electric vehicles and prolonging run-time of portable devices have brought more and more attention to high-energy-density energy storage devices. Besides, longer service life, higher specific energy density and lower production cost have always been the motivation for the scientific development (R. Schmuch et al., 2018). Silicon (Si) is considered as anode materials for next generation of high-energy-density lithium-ion batteries (LIBs) due to its high theoretical specific capacity of 4200 mAh g^{-1} (Y. Li et al., 2016, M. Ashuri et al., 2018). However, the huge volume change of silicon during lithiation/delithiation (> 300%) would bring about a series of problems, such as mechanical stress, loss of connection between particles and conductive matrix, continuous formation of solid-electrolyte interface (SEI) layer, all of which would ultimately result in rapid capacity decay and poor cycling

performance (Q. Xu et al., 2017 M.T. McDowell et al., 2013). Despite the successful implementation of nanostructured silicon such as nanoparticles and nanowires as anode materials, has been proved to be efficacious for reducing the volume change, however, the inherent volume variation and low electrical conductivity of silicon thwarted their commercial application (J. Wang et al., 2015, N. Liu et al., 2014). Theoretically, porous silicon with engineered pore size, which would act as buffer against the expansion of active material, and high conductivity, which is achieved by appropriate coating layer such as carbon, could result in higher delivered capacity and longer cycling life (H. Zhou et al., 2014 Y.-C. Zhang et al., 2016, B. Jiang et al., 2016). But the possibility of long-term cycling is limited, due to the weak interfacial bonding between carbon and silicon and the low mechanical strength., (X. Bai et al., 2016). The construction of a buffer layer at the interface of Si@C composites is considered to be an effective way to address this issue (C. Hoeltgen et al., 2016), however, the side reactions between the buffer layer and electrolyte during cycling is not conducive to the stability and efficiency of the electrode. Therefore, it is critical and imperative to design silicon anode with high energy density and controlled volume change, through a cost-effective and scalable synthesis method.

This study reports the synthesis of a double-layer stable coral-like porous silicon as a high-performance anode material for lithium-ion batteries. Low cost microsilica was used as raw material by low temperature magnesium thermal reduction technology and oxidation control and polymer carbonization treatment (W. Luo et al., 2011). The nano-porous silicon anode material with coral-like structure (PSi@C(N)) has excellent electrochemical properties and is an ideal anode material for lithium-ion batteries due to its simple and economical preparation method. In addition, the developed method provides a high value-added utilization strategy for semiconductor and photovoltaic waste recovery, in line with the global green energy movement.

Results And Discussion

The synthesis route of the PSi@C(N) anode material and the characterization of key intermediates are summarized in Fig. 1a. The Mg_2Si particles were prepared at 650°C by mixing Mg, microsilica and NaCl. After the removal of Mg by HCl washing, the porous silicon particles were coated with a layer of RF resin polymer by sol-gel method, and then carbonized under nitrogen atmosphere. The XRD patterns (Fig. 1b) confirmed the success of each synthesis step. The disappearance of SiO_2 peaks and the appearance of Mg_2Si peak (JCPDS card No. 36–0773) (M. Chen et al., 2018), indicated that the precursors of the powders were completely converted into Mg_2Si. The pattern of the final material PSi@C(N) suggested the successful removal of MgO and NaCl, as well as the existence of silicon (JCPDS card No. 27-1402) (W. Wu et al., 2016). Noted the peak narrowing of PSi@C(N) was attributed to lattice deformation due to stress generated in the surrounding the Si atom network after nitrogen doping (M. Ashuri et al., 2020). To further prove the existence of carbon-coating, Raman spectra were employed (Fig. 1c). The peak centered at ~ 510 cm^{-1} stood for the silicon Raman phonon vibration. In addition, the two peaks located at 1342 cm^{-1} and 1589 cm^{-1}, corresponding to the D and G bands of carbon materials, respectively, which indicated the formation of the carbon coating layer (Y. Cheng et al., 2016).

The porous microstructure of microsilica and PSi@C(N) were studied by nitrogen adsorption-desorption analysis. The specific surface area values were calculated from the Barrett-Emmett-Teller (BET) method, while pore volume and pore size distribution were computed by the Barrett-Joyner-Halenda (BJH) method (Fig. S2 and Table S2). Microsilica particles displayed relatively low specific surface area (22.225 $m^2 g^{-1}$) and low pore volume (0.080 $cm^3 g^{-1}$). In contrast, PSi@C(N) particles exhibited higher surface area (63.942 $m^2 g^{-1}$) with larger pore volume (0.265 $cm^3 g^{-1}$). The tight carbon-coating structure on the outer layer of PSi@C(N) resulted in a decrease in the pore size from 4.256 nm to 3.385 nm. The developed porous microstructure with high specific surface area is favorable for Li^+ ions migration and can effectively relieve structural stress roots from cycling (J.R. Matos et al., 2003).

XPS is employed to analyze the individual components of composites (Fig. 1d-1e). There are three main peaks in the high-resolution XPS spectra of Si 2p, of which the peaks at 101.5 eV and 103.5 eV are attributed to the Si $2p^{1/2}$ and Si $2p^{3/2}$ of Si, respectively, while the characteristic peaks of Si-O-Si bond of SiO_x at 100.8 eV correspond to Si-O-Si (Y. Xiao et al., 2014). This has demonstrated that, SiO_x is present on the surface of silicon particles. The C 1s spectrum has been deconvoluted into three distinct peaks, the peaks at 284.5 eV, 286.2 eV and 282.5 eV, which corresponds to the sp2 carbon atom, C-O bond and C-Si bond, respectively. This indicates the presence of graphitic carbon (M. Xia rt al., 2020), and there is a small amount of SiC is formed at the interface between Si and C during the process of high temperature carbonization (H. Tang et al., 2015) .that. The N 1s spectrum (Fig. 1f) contains two sets of peaks. The peaks at 395.5.8 eV and 398.5 eV, which stands for the N_2 and Si_3N_4 phases. In conclusion, the XPS analysis results have further confirmed the successful synthesis of PSi@C(N) nanocomposites. The TGA measurement (Fig. S2) revealed a mass loss of 9.62 wt%, caused by the oxidation of the carbon layer.

The microstructure and morphology of the products were examined by SEM and TEM. The microsilica particles exhibit spherical morphology with particle diameter ranging between 100 to 500 nm (Fig. 2a). After magnesiothermic reduction, the forming Mg_2Si particles does not show any particular morphology (Fig. 2b). Oxidative acid etching results in a formation of a porous Si nanoparticles with fluffy morphology, as shown in Fig. 2c. Silicon nanoparticles with diameter ranging from 100 to 200 nm are beneficial for fast diffusion of Li^+ ions (Fig. 2d), while a thin SiO_x layer (~ 5 nm), which is formed around the porous Si nanoparticles, can effectively alleviate the stress caused by the volume change of silicon particles during the cycling (Fig. 2e) (D. Chen et al., 2012, X F.-F Cao et al.,2011, S. Zhang et al., 2010). After carbon coating, PSi@C(N) particles with primary nano building blocks and many void spaces are formed (Fig. 2f). Elemental mapping confirms the presence of N-doped carbon layer (Figs. 2g-2j). This carbon layer improves the electronic conductivity of material and prolongs the cycle life of electrode (N. Liu et al., 2012).

In order to evaluate the electrochemical performance of the as-prepared PSi@C(N) particles as active material, half cells with Li chip as reference electrode were fabricated. The specific capacity was normalized to the total weight of PSi@C(N) material. The PSi@C(N) electrode was pre-lithium after 10 initial cycles at 200 mAh g^{-1}, and its performance was tested in a long-term cycle at 1000 mA g^{-1} (Fig.

3a). The PSi@C(N) electrode delivers 803.92 mAh g^{-1} after 300 cycles, which is ~ 60% of the initial capacity. This is much higher than both microsilica and porous silicon (Fig. 3b). The capacity of microsilica electrode is below 300 mAh g^{-1} because silica is a poor conductor. Porous silicon has delivered higher capacity, 1024.21 mAh g^{-1} after 50 cycles. This is attributed to nanoscale size effect and porous structure of PSi, which leaves plenty of room for the silicon to expand in volume during charging. The cycling stability of the PSi anodes is further improved by carbon coating. The reversible capacity of PSi@C(N) anodes is 1304.6 mAh g^{-1} after 50 cycles. Figure 3c shows the voltage distribution of PSi@C(N) electrode to Li^+/Li between 0.01 and 2 V at a current density of 1000 mA g^{-1}. The initial discharge and charge capacities are 1302.4 and 1075.6 mAh g^{-1}, respectively. The corresponding initial Coulomb efficiency (ICE) is 76.92%. After 5 cycles, the C.E. gradually increases to 98%, indicating the formation of stable SEI layer and reversible Li^+ storage (S. Weckend et al.,2016, J. Cui et al., 2017). Rate capability testing results of PSi@C(N) electrode are presented in Fig. 3d. By step-wise increasing the current density from 200 mA g^{-1} to 4000 mA g^{-1}, the average capacity was increased from 1957.2 to 1209.3 mAh g^{-1}. When the current rate is switched back to 200 mA g^{-1}, the reversible capacity is restored to 1892.9 mAh g^{-1}. Cyclic voltammetry (CV) measurements at the PSi@C(N) electrode were made in the range of 0.01 to 2.0 V at a scanning rate of 0.1 mV s^{-1}, as shown in Fig. 4e. In the first cycle, a wide cathode peak at ~ 0.6V appears, which is not detected in the following cycles. We attribute this peak to SEI membrane formation, which is an irreversible reaction. The peak observed at ~ 0.2V is related to the alloying reaction between lithium and silicon, which is consistent with the charge-discharge curve (L. Su et al., 2015, M. Gu et al., 2015). The anodic peaks of Li_xSi at 0.35 V and 0.5 V belong to the dealloying process respectively (J. Kong et al.,2013).

Figure 4 shows the electrode kinetics of the preparation of key materials for each component in the synthesis process. Figure 4(a, b, c, S4) shows the EIS spectra of microsilicon, porous silicon and PSi@C(N) electrodes as well as the fitting lithium-ion diffusion coefficient, which proves that the composite electrode has high lithium-ion diffusion ability and low resistance. Figure 4(d, e, f) shows the CV curves of PSi@C(N) electrodes at different scanning rates and the calculation of battery properties. The results indicate that capacitive behavior plays a dominant role in the storage and release of lithium ions at high scanning rates. The introduction of N doping layer enhances the connection between electrolyte and active material and improves the pseudocapacitive behavior (V. Augustyn et al., 2014). Figure 4(g, h, i) illustrates the diffusion behavior of lithium ions by Galvanostatic Intermittent Titration Technique (GITT). The three dynamics fully explain the effective contribution of each component of the composite to the overall click. The electrode with PSi@C(N) as active material has better dynamic behavior.

To further investigate the effect of the materials design on the performance of the electrode, coin cells were disassembled after 100 cycles and PSi@C(N) electrodes were extracted and examined under SEM (Figs. S5b-S5c). The measured thickness of the coated material on the fresh electrode is ~ 43 μm. After 100 charge/discharge cycles, the thickness is increased to ~ 51 μm (18.6% increase). Considering the huge volume change of silicon in lithiation/delithiation process, as depicted in Fig. S5a, we can relate the

small increase in the electrode thickness to the unique design of PSi@C(N) composites. The uniform distribution of nanocrystalline silicon inside the matrix has inhibited the inhomogeneous expansion, and thus the structural porosities reserve sufficient space for the silicon expansion and maintain the integrity of the electrode for several cycles. The stringent SiO_x layer formed around the core, acts like a cushion, which could harness volume expansion of silicon and preserve the structural integrity of the electrode. Furthermore, the N-doped carbon shell promotes the electronic conductivity of the electrode and shortens the diffusion path of Li^+ ions. In addition, the carbon layer prevents the vigorous side reactions between electrode and electrolyte at the interface. Therefore, it is concluded that, a steady SEI layer is formed around the active materials (F. Xi et al., 2021).

Conclusions

In summary, a Coral-like PSi@C(N) composite with superior properties have been successfully synthesized through a magnesiothermic reaction between microsilica and magnesium powder followed by carbon coating at elevated temperatures. As an anode candidate for Li-ion batteries, this material delivers an initial capacity of 1388.44 mAh g^{-1}, and a reversible capacity of 803.92 mAh g^{-1} after 300 deep charge/discharge cycles at 1000 mA g^{-1}. The change in the active material thickness on the electrode is recorded as 18.6%. This electrochemical performance is attributed to the engineered design of PSi@C(N). The silicon content is evenly distributed inside the core. The SiO_x buffer layer, which is formed around the silicon core, is able to assist in the minimization of the lithiation-induced volume change, and prevent the formation of cracks in the electrodes. The nitrogen-doped carbon coating boosts the electronic conductivity of the composites and facilitated Li^+ ions transport to the electrode. Benefitting from the synergistic effects of the evenly distributed silicon matrix, SiO_x buffer rigid layer, and N-doped carbon shell, a stable SEI layer is formed around PSi@C(N) active material. This study demonstrates a simple and cost-effective method for the preparation of anode materials for the new generation of high-performance lithium-ion batteries. In addition, it provides a feasible scheme for the high added-value use of microsilica, which is in line with the global sustainable development strategy.

Declarations

Acknowledgments

Financial support of this work from the National Natural Science Foundation of China (Grant No. 51974143, 51904134, 52164050, 51762043); National Key R&D Program of China (No. 2018YFC1901801, No. 2018YFC1901805); Major Science and Technology Projects in Yunnan Province (No. 2019ZE007, 202102AB080016, 202103AA08000); Yunnan Ten Thousand Talents Project (YNWR-QNBJ-2018-111), the Program for Innovative Research Team in University of Ministry of Education of China (No. IRT_17R48), Guiding Project of Scientific Research Program in Ministry of Education of Hubei Province (No. B2021025) and High-level Talent Project of Wuhan University of Science and Technology (Grant No. 101/1010071).

References

1. Armand M, Tarascon J-M (2008) Building better batteries. Nature 451(7179):652–657. https://doi.org/https://doi.org/10.1038/451652a
2. Qing Y, Zenan Z, Deyu K, Rongshen C (2007) Influence of nano-SiO_2 addition on properties of hardened cement paste as compared with silica fume. Constr Build Mater 21(3):539–545. https://doi.org/https://doi.org/10.1016/j.conbuildmat.2005.09.001
3. Poon CS, Kou SC, Lam L (2006) Compressive strength, chloride diffusivity and pore structure of high performance metakaolin and silica fume concrete. Constr Build Mater 20(10):858–865. https://doi.org/https://doi.org/10.1016/j.conbuildmat.2005.07.001
4. Prasanya D, Vignesh S, Gurulakshmi R (2016) Effects of fiber and silica fume characteristics on mechanical properties of high-strength concrete. Int Res J Eng Technol (IRJET) 3(5):3177–3181
5. Wongkeo W, Thongsanitgarn P, Poon C-S, Chaipanich A (2019) Heat of hydration of cement pastes containing high-volume fly ash and silica fume. J Therm Anal Calorim 138(3):2065–2075. https://doi.org/10.1007/s10973-019-08641-7
6. Yazıcı H (2008) The effect of silica fume and high-volume Class C fly ash on mechanical properties, chloride penetration and freeze–thaw resistance of self-compacting concrete. Constr Build Mater 22(4):456–462. https://doi.org/https://doi.org/10.1016/j.conbuildmat.2007.01.002
7. Pelisser F, Zavarise N, Longo TA, Bernardin AM (2011) Concrete made with recycled tire rubber: Effect of alkaline activation and silica fume addition. J Clean Prod 19(6):757–763. https://doi.org/https://doi.org/10.1016/j.jclepro.2010.11.014
8. Schmuch R, Wagner R, Hörpel G, Placke T, Winter M (2018) Performance and cost of materials for lithium-based rechargeable automotive batteries. Nat Energy 3(4):267–278. https://doi.org/10.1038/s41560-018-0107-2
9. Li Y, Yan K, Lee H-W, Lu Z, Liu N, Cui Y (2016) Growth of conformal graphene cages on micrometre-sized silicon particles as stable battery anodes. Nat Energy 1(2):15029. https://doi.org/10.1038/nenergy.2015.29
10. Ashuri M, He Q, Shaw LL (2016) Silicon as a potential anode material for Li-ion batteries: where size, geometry and structure matter. Nanoscale 8(1):74–103. https://doi.org/10.1039/C5NR05116A
11. Xu Q, Li J-Y, Sun J-K, Yin Y-X, Wan L-J, Guo Y-G (2017) Watermelon-Inspired Si/C Microspheres with Hierarchical Buffer Structures for Densely Compacted Lithium-Ion Battery Anodes. Adv Energy Mater 7(3):1601481. https://doi.org/https://doi.org/10.1002/aenm.201601481
12. McDowell MT, Lee SW, Harris JT, Korgel BA, Wang C, Nix WD, Cui Y (2013) In Situ TEM of Two-Phase Lithiation of Amorphous Silicon Nanospheres. Nano Lett 13(2):758–764. https://doi.org/10.1021/nl3044508
13. Wang J, Meng X, Fan X, Zhang W, Zhang H, Wang C (2015) Scalable Synthesis of Defect Abundant Si Nanorods for High-Performance Li-Ion Battery Anodes. ACS Nano 9(6):6576–6586. https://doi.org/10.1021/acsnano.5b02565

14. Liu N, Lu Z, Zhao J, McDowell MT, Lee H-W, Zhao W, Cui Y (2014) A pomegranate-inspired nanoscale design for large-volume-change lithium battery anodes. Nat Nanotechnol 9(3):187–192. https://doi.org/10.1038/nnano.2014.6
15. Zhou H, Nanda J, Martha SK, Unocic RR, Meyer HM, Sahoo Y, Miskiewicz P, Albrecht TF (2014) Role of Surface Functionality in the Electrochemical Performance of Silicon Nanowire Anodes for Rechargeable Lithium Batteries. ACS Appl Mater Interfaces 6(10):7607–7614. https://doi.org/10.1021/am500855a
16. Zhang Y-C, You Y, Xin S, Yin Y-X, Zhang J, Wang P, Zheng X-s, Cao F-F, Guo Y-G (2016) Rice husk-derived hierarchical silicon/nitrogen-doped carbon/carbon nanotube spheres as low-cost and high-capacity anodes for lithium-ion batteries. Nano Energy 25:120–127. https://doi.org/https://doi.org/10.1016/j.nanoen.2016.04.043
17. Jiang B, Zeng S, Wang H, Liu D, Qian J, Cao Y, Yang H, Ai X (2016) Dual Core–Shell Structured Si@SiO_x@C Nanocomposite Synthesized via a One-Step Pyrolysis Method as a Highly Stable Anode Material for Lithium-Ion Batteries. ACS Appl Mater Interfaces 8(46):31611–31616. https://doi.org/10.1021/acsami.6b09775
18. Bai X, Yu Y, Kung HH, Wang B, Jiang J (2016) Si@SiO_x/graphene hydrogel composite anode for lithium-ion battery. J Power Sources 306:42–48. https://doi.org/https://doi.org/10.1016/j.jpowsour.2015.11.102
19. Hoeltgen C, Lee J-E, Jang B-Y (2016) Stepwise carbon growth on Si/SiO_x core-shell nanoparticles and its effects on the microstructures and electrochemical properties for high-performance lithium-ion battery's anode. Electrochim Acta 222:535–542. https://doi.org/https://doi.org/10.1016/j.electacta.2016.11.006
20. Luo W, Wang Y, Chou S, Xu Y, Li W, Kong B, Dou SX, Liu HK, Yang J (2016) Critical thickness of phenolic resin-based carbon interfacial layer for improving long cycling stability of silicon nanoparticle anodes. Nano Energy 27:255–264. https://doi.org/https://doi.org/10.1016/j.nanoen.2016.07.006
21. Chen M, Li B, Liu X, Zhou L, Yao L, Zai J, Qian X, Yu X (2018) Boron-doped porous Si anode materials with high initial coulombic efficiency and long cycling stability. J Mater Chem A 6(7):3022–3027. https://doi.org/10.1039/C7TA10153H
22. Wu W, Zhang J, Fan W, Li Z, Wang L, Li X, Wang Y, Wang R, Zheng J, Wu M, Zeng H (2016) Remedying Defects in Carbon Nitride To Improve both Photooxidation and H2 Generation Efficiencies. ACS Catal 6(5):3365–3371. https://doi.org/10.1021/acscatal.6b00879
23. Ashuri M, He Q, Shaw LL (2020) Improving cycle stability of Si anode through partially carbonized polydopamine coating. J Electroanal Chem 876:114738. https://doi.org/https://doi.org/10.1016/j.jelechem.2020.114738
24. Cheng Y, Yi Z, Wang C, Wang L, Wu Y, Wang L (2016) Influence of copper addition for silicon–carbon composite as anode materials for lithium ion batteries. RSC Adv 6(62):56756–56764. https://doi.org/10.1039/C6RA12332E

25. Matos JR, Kruk M, Mercuri LP, Jaroniec M, Zhao L, Kamiyama T, Terasaki O, Pinnavaia TJ, Liu Y (2003) Ordered Mesoporous Silica with Large Cage-Like Pores: Structural Identification and Pore Connectivity Design by Controlling the Synthesis Temperature and Time. J Am Chem Soc 125(3):821–829. https://doi.org/10.1021/ja0283347
26. Xiao Y, Wang X, Xia Y, Yao Y, Metwalli E, Zhang Q, Liu R, Qiu B, Rasool M, Liu Z, Meng J-Q, Sun L-D, Yan C-H, Müller-Buschbaum P, Cheng Y-J (2014) Green Facile Scalable Synthesis of Titania/Carbon Nanocomposites: New Use of Old Dental Resins. ACS Appl Mater Interfaces 6(21):18461–18468. https://doi.org/10.1021/am506114p
27. Xia M, Chen B, Gu F, Zu L, Xu M, Feng Y, Wang Z, Zhang H, Zhang C, Yang J (2020) $Ti_3C_2T_x$ MXene Nanosheets as a Robust and Conductive Tight on Si Anodes Significantly Enhance Electrochemical Lithium Storage Performance. ACS Nano 14(4):5111–5120. https://doi.org/10.1021/acsnano.0c01976
28. Tang H, Xia XH, Zhang YJ, Tong YY, Wang XL, Gu CD, Tu JP (2015) Binary conductive network for construction of Si/Ag nanowires/rGO integrated composite film by vacuum-filtration method and their application for lithium ion batteries. Electrochim Acta 180:1068–1074. https://doi.org/https://doi.org/10.1016/j.electacta.2015.09.032
29. Chen D, Mei X, Ji G, Lu M, Xie J, Lu J, Lee JY (2012) Reversible Lithium-Ion Storage in Silver-Treated Nanoscale Hollow Porous Silicon Particles. Angew Chem Int Ed 51(10):2409–2413. https://doi.org/https://doi.org/10.1002/anie.201107885
30. Cao F-F, Deng J-W, Xin S, Ji H-X, Schmidt OG, Wan L-J, Guo Y-G (2011) Adv Mater 23(38):4415–4420. https://doi.org/https://doi.org/10.1002/adma.201102062. Cu-Si Nanocable Arrays as High-Rate Anode Materials for Lithium-Ion Batteries
31. Zhang S, Du Z, Lin R, Jiang T, Liu G, Wu X, Weng D (2010) Nickel Nanocone-Array Supported Silicon Anode for High-Performance Lithium-Ion Batteries. Adv Mater 22(47):5378–5382. https://doi.org/https://doi.org/10.1002/adma.201003017
32. Liu N, Wu H, McDowell MT, Yao Y, Wang C, Cui Y (2012) A yolk-shell design for stabilized and scalable Li-ion battery alloy anodes. Nano Lett 12(6):3315–3321
33. Weckend S, Wade A, Heath GA (2016) End of life management: solar photovoltaic panels, National Renewable Energy Lab.(NREL), Golden, CO (United States),
34. Cui J, Cheng F, Lin J, Yang J, Jiang K, Wen Z, Sun J (2017) High surface area C/SiO_2 composites from rice husks as a high-performance anode for lithium ion batteries. Powder Technol 311:1–8. https://doi.org/https://doi.org/10.1016/j.powtec.2017.01.083
35. Su L, Xie J, Xu Y, Wang L, Wang Y, Ren M (2015) Preparation and lithium storage performance of yolk-shell Si@void@C nanocomposites. Phys Chem Chem Phys 17(27):17562–17565. https://doi.org/10.1039/C5CP01954K
36. Gu M, Ko S, Yoo S, Lee E, Min SH, Park S, Kim B-S (2015) Double locked silver-coated silicon nanoparticle/graphene core/shell fiber for high-performance lithium-ion battery anodes. J Power Sources 300:351–357. https://doi.org/https://doi.org/10.1016/j.jpowsour.2015.09.083

37. Kong J, Yee WA, Wei Y, Yang L, Ang JM, Phua SL, Wong SY, Zhou R, Dong Y, Li X, Lu X (2013) Silicon nanoparticles encapsulated in hollow graphitized carbon nanofibers for lithium ion battery anodes. Nanoscale 5(7):2967–2973. https://doi.org/10.1039/C3NR34024D
38. Liu H, Shan Z, Huang W, Wang D, Lin Z, Cao Z, Chen P, Meng S, Chen L (2018) Self-Assembly of Silicon@Oxidized Mesocarbon Microbeads Encapsulated in Carbon as Anode Material for Lithium-Ion Batteries. ACS Appl Mater Interfaces 10(5):4715–4725. https://doi.org/10.1021/acsami.7b16760
39. Augustyn V, Simon P, Dunn B (2014) Pseudocapacitive oxide materials for high-rate electrochemical energy storage. Energy Environ Sci 7(5):1597–1614. https://doi.org/10.1039/C3EE44164D
40. Xi F, Zhang Z, Hu Y, Li S, Ma W, Chen X, Wan X, Chong C, Luo B, Wang L (2021) PSi@SiO_x/Nano-Ag composite derived from silicon cutting waste as high-performance anode material for Li-ion batteries. J Hazard Mater 414:125480. https://doi.org/https://doi.org/10.1016/j.jhazmat.2021.125480

Figures

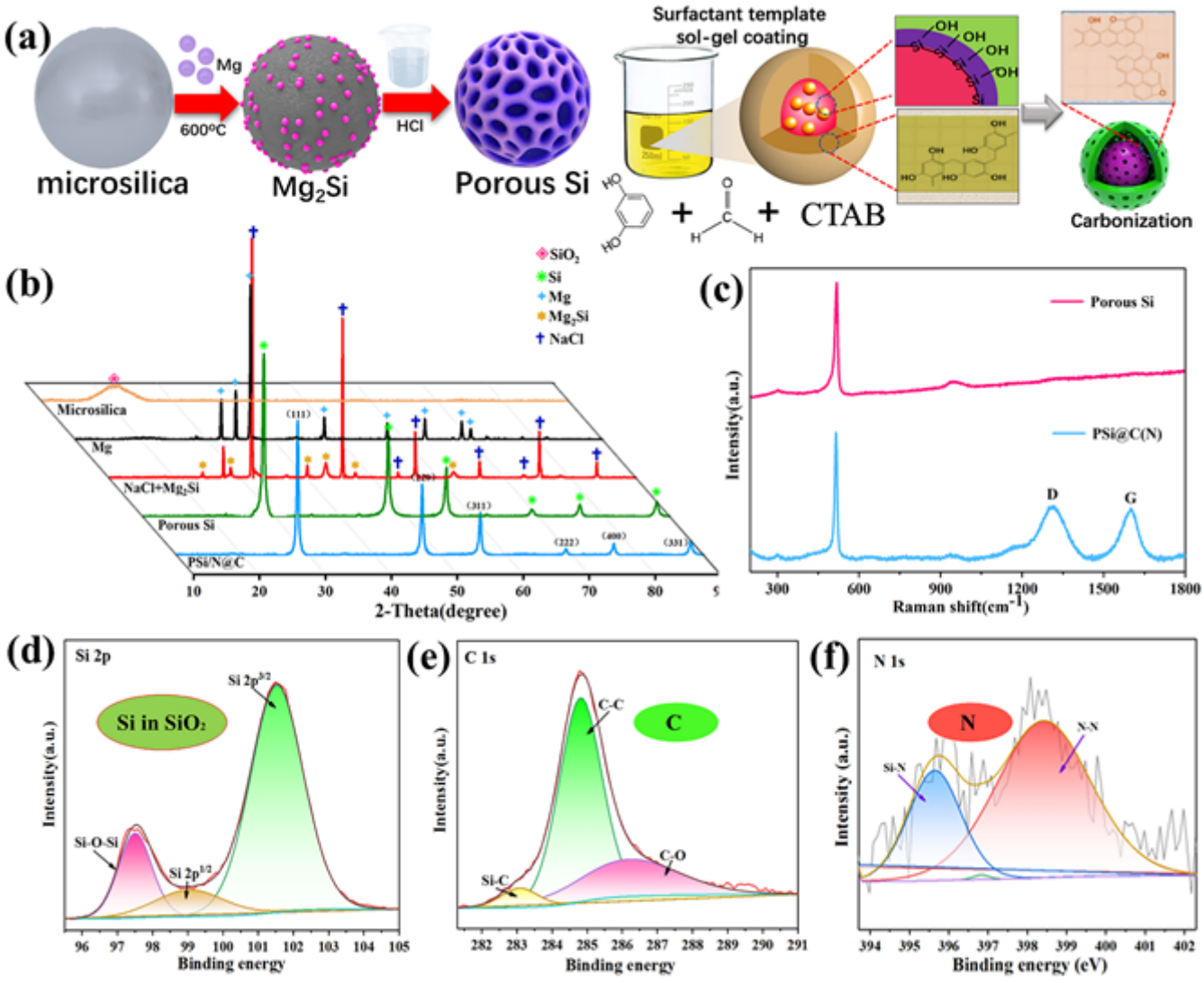

Figure 1

(a) Schematic illustration of the synthesis of PSi@C(N), (b) XRD patterns, (c) Raman spectra, and (d) XPS spectra of PSi@C(N), (d) Si 2p, (e) C 1s, (f) N 1s.

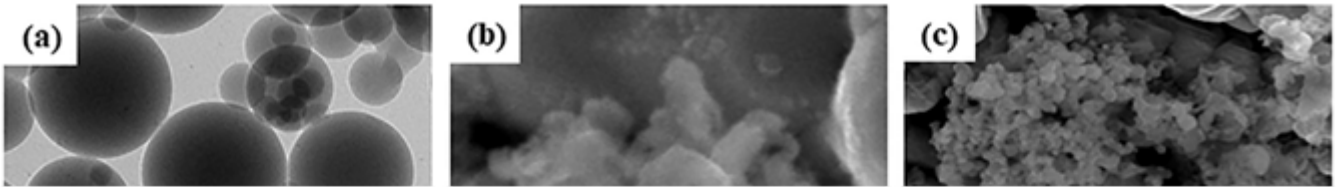

Figure 2

(a) TEM image of microsilica particles, (b) SEM image of Mg_2Si, (c-e) SEM and HRTEM images of porous Si nanoparticles collected after magnesiothermic reduction, (f-j) SEM image of PSi@C(N) particles along with elemental mapping (g-j).

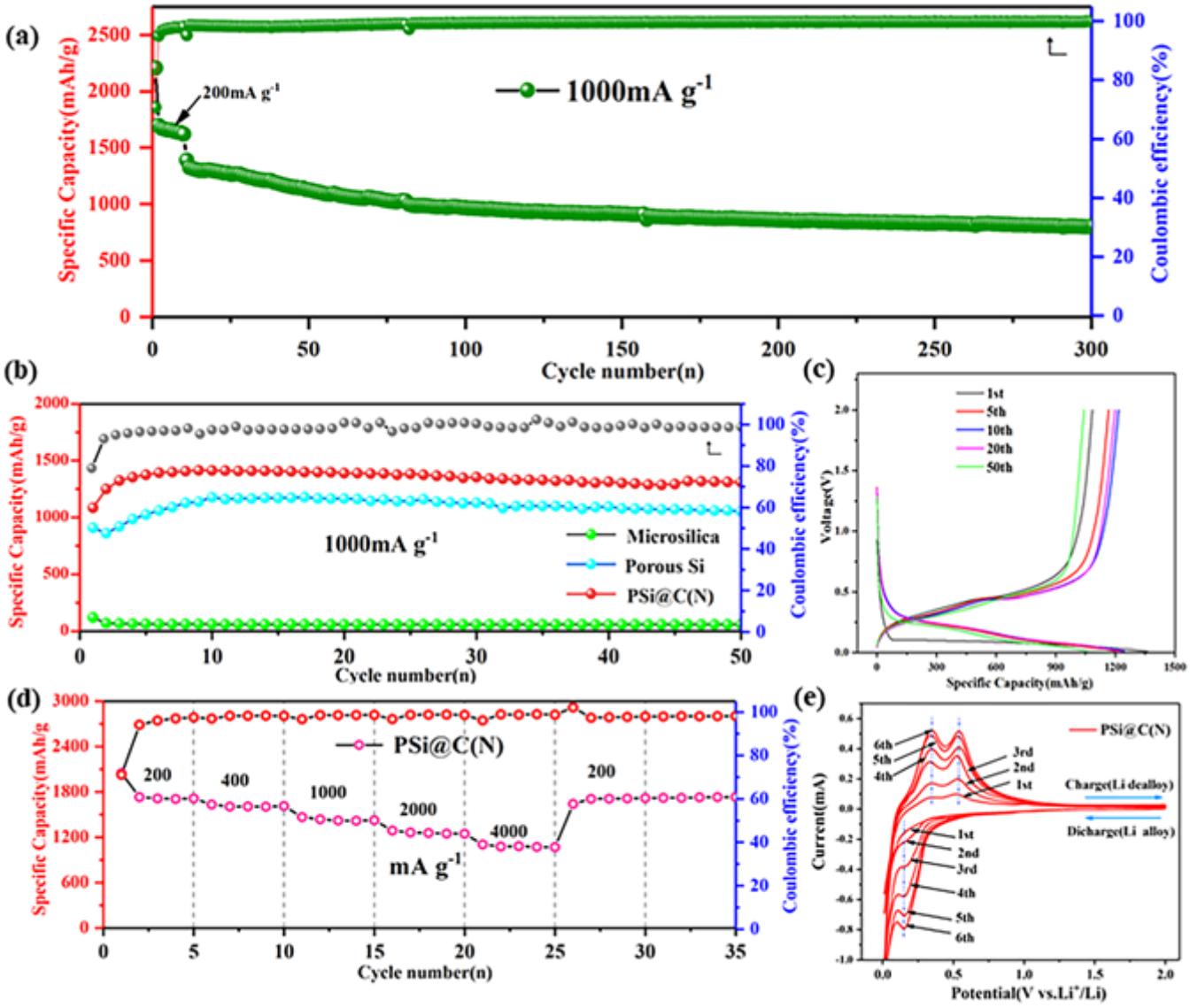

Figure 3

(a) Electrochemical cycling results of PSi@C(N) electrodes. (a) Delithiation capacity and Coulombic efficiency for 300 cycles at 1000 mA g^{-1}, (b) comparison between galvanostatic cycling performance of microsilica, porous Si (PSi) and PSi@C(N), (c) voltage profiles of PSi@C(N) electrode plotted for selected cycles (1000 mA g^{-1}), (d) rate retention test of the PSi@C(N) electrode at various rates, and (e) cyclic voltammograms for PSi@C(N) from 0.01 V to 2.0 V vs. Li+/Li at a scan rate of 0.1 mV s^{-1}.

Figure 4

(a) Nyquist plots as well as (b) linear fitting of Z' vs. $\omega^{-1/2}$ plots and (c) apparent diffusion coefficients of the microsilica, PSi, and as-prepared PSi@C(N) composites electrodes. (d) CV curves at different scan rates as well as (e) fitted lines and log (i) vs. log (v) plots at oxidation and reduction peaks, and (f)

capacity contribution at different scan rates calculation of the as-prepared PSi@C(N) composites electrode. (g) GITT curves of the PSi@C(N) electrode (discharge/charge state), (h) E vs. t profile for one GITT test, (i) I vs t profile for one GITT test.

Supplementary Files

This is a list of supplementary files associated with this preprint. Click to download.

- SupportingInformation.docx